Derivation of SOL Transport Coefficients Using 2D Modelling for Hot-Ion ELM-Free H-Modes in JET

G. K. McCormick*, A. Chankin, S. Clement, S. Davies, J. Ehrenberg,
A. Loarte, R. Monk, R. Simonini, J. Spence, M. Stamp, A.Taroni, G. Vlases

JET Joint Undertaking, Abingdon, Oxfordshire, OX14 3EA, United Kingdom
* Max-Planck-Institut für Plasmaphysik, Boltzmannstr. 2, 85748 Garching, Germany

ABSTRACT

Profiles of J_{sat} and T_e measured by Langmuir probes at the target plates of the JET MkI divertor, and the target plate power loading are modelled using the EDGE2D/NIMBUS codes assuming perpendicular particle transport via diffusion alone or with a pinch. The low-density ($\bar{n}_e$~$1x10^{19}m^{-3}$) OH plasma preceding high-power NBI, as well as the ELM-free high performance H^* and high performance rollover H^{RO} phases are considered. The power splitting between ions P_i (≥7MW) and electrons P_e (<1MW) in conjunction with the H-mode transport barrier effect that J_{sat} and T_e change little from OH to H^* conditions, although P_{in} ~20MW and $\bar{n}_e$ increases a factor of three. Power balance is good. χ_i is taken as $1m^2/s$. χ_e varies from the strike point outwards as ~0.5-$3m^2/s$ in all phases. $D_\perp$~0.03→0.015 m^2/s (OH→H*), or $v_{pinch}/D_\perp$ ~15→45→$25m^{-1}/s$ (OH→H^*→H^{RO}) with $D_\perp = 0.1m^2/s$. Sensitivity studies involving deep and shallow computational grids, wall material, different recycling scenarios, thermal transport barrier, and density scalings are carried out to judge the possible influence on derived transport coefficients.

1.INTRODUCTION

The ELM-free hot-ion H-mode is the mainstay of the JET D-T campaign and, in addition, represents an extreme corner of low-recycling SOL/divertor operational/modelling space. A marked difference in accessibility to this regime existed between the Single-Null-Up (SNU) dump-plate configuration of 1991-92 and the MkI divertor of 1994-95: Whereas ELMs on SNU were an exception, type I ELMy H-modes were a natural feature of MkI. Only through dedicated experiments leading to minimal recycling conditions as well as optimization of triangularity and edge shear could a satisfactor ELM-free situation be recovered /1/.

On JET the duration of the ELM-free period appears dictated by the edge pressure gradient approaching ballooning or kink instability limits /2/. The rate of formation of this gradient seems correlated with the level of recycling, and thus implicitly with the nature of plasma-wall interaction and shielding efficiency of the edge/SOL plasma against recycling

neutrals. Since attainment and sustenance of the ELM-free period is vital for the success of JET D-T operation and generally for VH-modes, and because analysis of the ELM-free situation can provide insights as to the nature of those processes leading to the breakdown of the edge transport barrier via an ELM or outer mode /1/, this modelling study is intended to establish a baseline for continuing code/machine-based investigations on control of these events.

In fig.1 the temporal development of a hot-ion H-mode is considered: An x-point is formed at 11.5 sec leading to a density pumpout of the OH target plasma. P_{NBI}~17.5MW is initiated at 12 sec where $\bar{n}_e$ (~$1x10^{19}m^{-3}$) is such that shine-through is limited to permissible levels (~30%). $\bar{n}_e$ then climbs at a rate corresponding to 40% faster than beam fuelling while neither the divertor D_α, J_{sat} to a target plate Langmuir probe or the subdivertor neutral pressure P_{SD} undergo significant changes from the OH phase. At 12.96 sec an outer mode provokes a temporal rollover in the D-D reaction rate R_{DD} and W_{dia}, leading to a prompt augmentation of flux to the target as registered in the D_α signal. In the pre-rollover phase $P_{loss} = P_{abs} + P_{OH} - dW_{dia}/dt - P_{rad}$ ~ 10MW. At the rollover, P_{loss} increases to ~16MW. Using a 1-D heat transport model, the rapid rise in target plate temperature indicates an approximate power loading of $P_{out}^{target} \geq 8MW$ and $P_{in}^{target} \geq 3MW$.

Table I summarizes configurational aspects and particle balances for the best high-performance shots of each setup. The particle balance between SNU and MkI is radically different: Although #26087 was accompanied by a gas puff in excess of beam fuelling, the rate of core density increase dN_e/dt was marginally above that dictated by the beams. Thus, the fuelling efficiency of the gas puff was only a few percent - in contrast to ~30% with MkI operation (on beryllium plates). Further, dN_e/dt for MkI was typically >30% above the beam fuelling rate, notwithstanding the more mechanically-closed divertor and cryopump. These differences may imply strongly pumping walls for #26087, or lower penetration efficiency past the transport barrier into the core plasma, or both. SOL calculations using $D_\perp$ derived from simulations here do not, however, indicate that any signifcant SOL shielding advantages should pertain to SNU.

2. EDGE2D SETUP AND EXPLORATORY INVESTIGATIONS

χ_e and $D_\perp$ are inferred by matching the outer target plate profiles of Jsat and Te. Other important code inputs are Pe and Pi, whose sum must be consistent with the overall power balance consisting of computed power to the target plates Ploss = Pabs + POH - dWdia/dt - Prad, and power to the target plates estimated from IR camera measurements.

2.1 Power Accountability

Due to the short ELM-free period (<1.3 sec) and technical aspects, few hot-ion H-mode discharges exist where IR camera measurements yield target plate power fluxes. In #34230 of

fig.2 one finds $P_{in}^{target} \sim P_{out}^{target}$, such that P_{total}^{target} ~6MW in the ELM-free phase and ~9.5MW at the rollover. Thus, on average, $P_{loss} - P_{total}^{target}$ ~2.8-4.5MW for H^* and ~1.5MW for H^{RO}. This latter number will actually be larger as W_{dia} does not resolve the short rollover phase. A P_{NBI} step-down discharge (#34236: 18.4→10MW) also yields $P_{in}^{target} \sim P_{out}^{target}$ ~3MW, with $P_{loss} - P_{total}^{target}$ ~1.5MW for H^*. Hence the indicated deficit between P_{loss} and P_{total}^{target} ranges over 1.5-4.5MW, not taking into account uncertainties involved in P_{NBI} (±1MW), P_{OH} (from neoclassical resistivity), P_{abs} (±0.5MW), P_{total}^{target} (±1MW) and dW_{dia}/dt. Since part of this deficit may originate from (CX) core losses not encompassed by the grid, P_{sol} ~ 7 MW (H^*) and ~12 MW (H^{RO}) are taken in detailed modelling.

2.2 Sensitivity Studies

More than 40 EDGE2D/NIMBUS runs have been performed to arrive at best fits for J_{sat} and T_{ed}, using $D_\perp$ alone or with a pinch, for three phases (OH, H^* and H^{RO}) of #32919. This shot was chosen as: a) it is the best HFE shot, b) acceptable target plate Langmuir probe data is available, and c) core parameters are excellently documented. The effects of different recycling scenarios, P_e-P_i power splitting, density scalings, thermal transport barrier, deep vs. shallow grids have been explored in order to judge consequences on derived transport coefficients and other experimentally-relevant code outputs.

The divertor substructure, including cryopump and bypasses to the main chamber are included, with the pumped neutrals being reintroduced into the main chamber as a uniform puff. Only one equilibrium grid is used to model the three phases, with a spatial exent of -0.4 or -9.5cm (deep core) to +1.8cm around the separatrix at the outer midplane. Diffusion alone, or with a pinch is assumed in modelling, constant on flux surfaces. Drifts are not considered. The upstream midplane density at the outer separatrix n_{es} as well as P_e and P_i are specified as inputs. A limit for ion momentun flux along field lines is employed/3/. Z_{eff}=1 is assumed. Z_{eff} ≥2 is probably more accurate ($Z_{eff} \leq 1.5$ in the core), which would lead to lower T_{ed} in the calculations. But then a full multi-fluid treatment needs be implemented - and this would have been too CPU time intensive for these studies. It is estimated that >50% of the typically 1MW of radiation in a hot-ion mode originates from Cu and Ni /4/, and the rest from carbon.

Detailed modelling uses a recycling coefficient R=1 with walls and target of CFC, i.e. a steady-state situation. Using the deep core (whose radial $\overline{n_e L}$ to the inner boundary was adjusted to roughly represent the experimental transport barrier), the particle flux passing through the inner grid boundary was allowed to accumulate at a rate 5×10^{20} s^{-1}, consistent with experiment. This loss was accommodated by either allowing R>1 or introducing an inner wall puff - both options being possible explanations for the recycling behavior extant in Table I. The computed profiles of J_{sat} and T_{ed} suffered only minor variations from the static case; thus, assuming R=1 should have little impact on deduced values of $D_\perp$ and χ_e.

About 2/3 of the main chamber walls facing the plasma consists of inconel. Perhaps more importantly, for SNU the inner wall was 100% graphite vs. 35% for MkI. One deep-core run with all-iron walls was performed to test the effect of deep-fuelling expected from the higher particle and energy reflection coefficients associated with metals: The SOL/divertor profiles changed little, but n_e at the inner grid increased by 25% while n_{es} was held constant - implying if enhanced core fuelling is an important aspect of exacerbating pressure-gradient-driven modes, then one may expect metallic walls to degrade high performance discharges, and probably H-mode quality in general. The complex of core neutral density and its relationship to metallic walls and potential effects on H-mode properties has been discussed elsewhere /5/.

If a constant χ_e is used in deep core calculations, equipartition is so strong between electrons and ions that the upstream T_{es} is always too large to be consistent with experimental downstream (divertor) T_{ed}, no matter what P_e is chosen within the relationship $P_e+P_i=7MW$. By allowing χ_e to vary spatially from smaller to larger values (0.1->0.4m^2/s, for example) from the inner core to the separatrix - thus augmenting the core temperature gradient - it was possible to depress T_{es} to a more reasonable level, while boosting predicted core T_e closer to that of experiment. Clearly, if an expanded core region is under scrutiny - with the H-mode in particular - it is necesssary to fully model the transport barrier as well as the SOL in order to make relevant statements. Since a sharp H-mode-like transport barrier is presently not implemented within EDGE2D, all calculations were done with the shallow core.

2.3 Other Considerations

χe is forced to vary as A + B/ne to better fit Ted profiles at the target plate. A and B are adjusted such that about the same χe profile results (~0.5-3m^2/s from the strike point outwards) regardless of ne. χi is held constant at 1m^2/s, for lack of better information.

Upstream parameters are not available for any HFE hot-ion H-mode shots. The neutral lithium beam diagnostic did probe similar discharges, indicating λ_{ne} referenced to the outer midplane was of the order 1cm /6/. RCP experience on SNU H-modes (1991) was λ_{ne} ~1$^+$cm. When modelling particle transport with a pinch and diffusion, the J_{sat} profile can be credibly fitted by adjusting $v_{pinch}/D_\perp$. $D_\perp$ may be selected to match λ_{neSOL}. For these studies $D_\perp$=0.1m^2/s was chosen, yielding λ_{neSOL} ~ 0.85 cm for the H* phase when $v_{pinch}/D_\perp$ = 45. This freedom to match upstream λ_{neSOL} and downstream λ_{Jsat} does not exist using diffusion alone.

3. EDGE2D/NIMBUS MODELLING OF #32919

Referring to fig.3, Langmuir probe profiles are modelled for the time slices: 51.75-52.0 sec (OH), 52.55-52.9 sec (H*) and 53.1-53.2 sec (H^{RO}). Salient results are summarized in Table

II. Table III summarizes the input parameters. Aside from OH where $P_e=P_i$ is assumed, P_e is selected ($P_e<<P_i$) to approximately reproduce T_{ed}, with the expectation that use of a realistic Z_{eff} will bring experimental and code T_{ed} profiles closer together. Half (estimated from experiment) of P_{rad} is radiated within the grid via a global carbon radiation function .

Code-experiment profile comparisons are shown in fig. 4-6. Inner-plate comparisons are not considered as the experimental profiles are not well-defined. We discuss density behavior first. For OH, essentially the same n_{es} ~ 0.55-0.6 x $10^{19}m^{-3}$ is required for both pure diffusion (PD) and the pinch to duplicate J_{sat}^{peak}, whereas for H*(PD) n_{es}~0.7x$10^{19}m^{-3}$ vs. 0.5 for H*(pinch). Even though J_{sat}^{peak} and n_{es} change little over OH→H*, the divertor density $n_{ed\ out}^{peak}$ drops a factor of two, this being related to $T_{id}>>T_{ed}$ in the H*-phase.

A marked difference in predicted upstream profiles is found: λ_{ne}^{sol}(PD, H*) ~0.5cm, which at a distance of 7mm from the separatrix then flattens to ~2.5cm. In contrast, λ_{ne}^{sol}(pinch, H*) ~0.84cm. In experiment, λ_{Jsat}^{div}(OH→H*) varies as 5.6→4 cm. To reproduce this, transport needs be changed as: $D_\perp$ = 0.03→0.015 m^2/s(PD) or $v_{pinch}/D_\perp$= 15→45 (pinch). The J_{sat} (H*) profiles computed using pure diffusion tend to turn unrealistically upwards at the outer edge of the grid. In contrast, pure diffusion better fits the private flux region, perhaps indicating that different transport laws are needed to describe different regions.

The rollover phase is modelled in an average sense by increasing $v_{pinch}/D_\perp$ to 25, and n_{es} to 0.85x$10^{19}m^{-3}$. $P_{sol}=P_e+P_i$=12.5MW is used to bring P_{total}^{target} into line with that observed in shots #34230 or #33641 (figures 1, 2). As P_{sol} increases, both CX neutrals and equipartition with electrons become more important loss channels for ion power (Table II).

Electron temperature profiles are broad in all three phases. The fits shown in fig.4-6 are achieved by allowing χ_e to increase from the strike point outwards, using a variant available within the code (χ_e= A+B/n_e) as described above. DIVIMP analysis also suggests χ_e changes spatially in this fashion /7/. The poor agreement between experiment and code in the private flux region is an artifact of using the n_e^{-1} scaling.

With respect to other quantities, the computed subdivertor pressure P_{SD} ~4x10^{-5}mbar during H* is typical of hot-ion H-modes. The code D_α at the target plates agree with experiment during OH, but are too low in the H-mode phase by 20-50%, even for the outer plate whose J_{sat} profile is reasonably modelled. D_α from molecules is not included in the code estimate, which will make up part of the difference. D_α^{horiz} arises from a horizontal viewing chord near the midplane which faces into the inner inconel wall. The code value is 30-50% of experiment. Code experience is that using metallic walls will increase D_α^{horiz} by 50%, and use of the deep core by another ~50%, so agreement with experiment is acceptable.

4. SUMMARY

Using EDGE2D/NIMBUS, the outer target J_{sat} and T_{ed} profiles and measured power to the plates have been modelled for the ELM-free and rollover phases, as well as the NBI-target OH plasma, of a low-recycling high performance discharge. These profiles undergo minor changes in passing from OH- to H^*-conditions, the difference being in power to the plate via the ions. Little NBI power is transmitted to the electron SOL, i.e. $P_i >> P_e$, and $T_{id} >> T_{ed}$. The H-mode transport barrier serves to isolate the divertor from dynamic activity of core where $\bar{n}_e$ can increase a factor of three during the ELM-free period with virtually no change in upstream density or particle flux to the target plate. Invariance of the SOL density profile during the H* phase has also been documented on ASDEX /8/. The rollover phase is modelled via an increase in perpendicular particle transport above H^*, about a factor of two increase in n_{es}, and augmentation in P_{sol} of perhaps 50%.

On JET an inwards pinch has been found useful in duplicating SOL parameters under high recycling conditions /9/. In the results presented here, pure diffusion produces distorted profiles in the far SOL under H^* conditions, because $D_\perp$ is very small. Use of a pinch permits larger $D_\perp$, as long as $v_{pinch}/D_\perp$ is adjusted correctly, resulting in predicted profiles fairly resiliant against recycling levels - which is observed experimentally in the hot-ion H-mode. Although $D_\perp \sim 0.1 m^2/s$ (in conjunction with a pinch) seems in accord with circumstantial experimental evidence, combined upstream-downstream measurements with the MkII divertor are necessary to make a convincing case for the absolute value of $D_\perp$, or for one form of transport or another.

$v_{pinch}/D_\perp = 15$ is a common value for L-mode plasmas /9/. $D_\perp = 0.03\ m^2/s$ is lower than $D_\perp \sim 0.05\ m^2/s$ (using $D_\perp$ constant on flux surfaces) /10/ found for higher-density OH conditions. $\chi_e \sim \chi_i \sim 1 m^2/s$ is typical of L-mode, but here λ_{Te}^{target} actually increases for OH→H*, necessitating $\chi_e(H^*, H^{RO}) > \chi_e(OH)$. This result is not sensitive to the exact value of χ_i.

The ratio $P_i/P_e > 10$ does not reflect the power splitting of the core, but that outside the transport barrier. Inclusion of the main plasma - in accord with the transport barrier - in a self-consistent manner with experimental parameters at the target plates is now being undertaken by combining the core transport code JETTO with EDGE2D/NIMBUS. This will enable power splitting to be addressed as well as estimate volume CX power losses not covered by the "thin-core" model used here. Out of 19MW injected, there is (on average) a difference of 3-4MW (H^*) between $P_{loss} = P_{abs} + P_{OH} - dW_{dia}/dt - P_{rad}$ and P_{target} (from the IR camera). Present calculations can account for $P_{CX} = 1.4$MW via CX neutrals - 70% occurring below the x-point - with P_{CX} being almost independent of n_{es}. Hence, even without inclusion of CX losses from the core, power accountability is reasonable.

SOL calculations using $D_\perp$ as derived for #32919 of MkI do not indicate any SOL shielding advantages should accrue to the SNU configuration of 1991. Thus, an explanation for the marked differences in particle balance between MkI and SNU must be sought elsewhere.

REFERENCES

/1/ T.C.C.Jones, et al., Plasma Physics and Contr. Fusion **37** (1995) A359

/2/ G.T.A.Huysmans, et al., Proc. 22nd EPS Conf. Bournemouth **19C** (1995) I-201

/3/ G.Radford, Contrib. Plasma Phys. **32** (1992) 297

/4/ K.Lawson, private communication, JET Joint Undertaking

/5/ K.Itoh and S-I.Itoh, Plasma Phys. Control. Fusion **37** (1995) 491

/6/ D.D.R.Summers, P.Breger, K.Erents, this conference

/7/ K.Erents, et al., this conference

/8/ G.K.McCormick, Z.A.Pietrzyk et al., J. Nucl. Mater. **176-177** (1990) 89

/9/ A. Taroni, et al., Proc. 22nd EPS Conf. Bournemouth **19C** (1995) IV-297

/10/ A.Loarte, et al., Proc. 22nd EPS Conf. Bournemouth **19C** (1995) III-305

ACKNOWLEDGMENTS

The authors gratefully acknowledge discussions and support from P.Andrew, A.Bickley, J.Christiansen, P.Coad, T.C.C.Jones, R.König, P.Lomas, D.Muir and R.Reichle.

Table I: Overview of global plasma properties and particle balances for the best high performance shots of each configuration.

Shot No. Configuration	**#26087** Single Null Up **SNU**	**#32919** High Flux Exp. **HFE MkI**	**#33643** Double-Null HFE **DNHF1 MkI**
x-pt height [m]	**0.084**	**0.15**	**0.15**
flux exp. inside	**17.6**	**12.5**	**13.6**
flux exp. outside	**15**	**8**	**10**
$I_p/B_t/q_{95}$	**3.2/2.8/3.7**	**3.1/3.45/4.0**	**3.9/3.45/3.4**
$\bar{n}_{e\ target}$ [m^{-3}]	**2.1×10^{19}**	**1.6×10^{19}**	**1.1×10^{19}**
R_{DD} [s^{-1}]	**8.4×10^{16}**	**7.6×10^{16}**	**9.3×10^{16}**
Particle Balance over 1st Sec. of NBI [$10^{21}s^{-1}$]			
$\int\Phi_{epump}dt$	**0**	**-0.41**	**-0.26**
$\int\Phi_{egas}dt$	**2.86**	**0**	**0.22**
$\int\Phi_{ebeam}dt$	**1.01**	**1.33**	**1.36**
δN_{etotal}	**1.06**	**1.80**	**2.0**
$\delta N_{etotal}/\int\Phi_{ebeam}dt$	**0.05**	**0.47**	**0.64**
$\delta N_e/\int\Phi_{ebeam}dt$	**1.05**	**1.36**	**1.47**

Table II: Summary of code and experimental values. "code"=code calc.with pinch;"diff"=pure diffusion

		OH		H*		H^{RO}	
		in	out	in	out	in	out
J_{sat}[A/cm^2]	expt.	?	6.3	10	7.4	~9-15	~9-16
	code	**7.1**	**5.8**	**7.8**	**7.7**	**12.6**	**12.3**
λ_{Jsat} [cm]	expt.	?	5.5	?	4.2	?	5.5
	code	**7.8**	**5.6**	**5.8**	**4.0**	**7.1**	**5.3**
T_{eD} [eV]	expt.	?	5.5	35	~50	33	~50
	code	**54**	**62**	**56**	**60**	**56**	**61**
λ_{TeD} [cm]	expt.	?	7.5	?	10	?	~10
	code	**8.5**	**6.7**	**12**	**8**	**11.4**	**8.2**
T_{iD} [eV]	**code**	**44**	**61**	**655**	**661**	**571**	**560**
n_{eD}[10^{19}m^{-3}]	code	0.64	0.48	0.27	0.26	0.46	0.44
n_{es} out. midp.	diff.	0.6		0.7		–	
[10^{19}m^{-3}]	pinch	0.55		0.5		~0.85	
λ_{neSOL}	diff.	1.1		0.53->2.5 at 7mm		–	
[cm]	pinch	1.43		0.84		1.26	
$q_{\|\|}$ [MW/m^2]	code	0.42	0.56	2.3	3.3	3.4	4.7
$\lambda_{q\|\|}$ [cm]		6.6	6.3	5.5	4.0	6.8	5.3
P_{targ} [MW]	code	0.59	0.74	2.44	2.94	4.1	5.0
$P_{i->e}$ [MW]	code	0.12		0.85		1.88	
P_{CX} [MW]	code	0.18 (60%)		1.4 (70%)		2.4 (77%)	
ϕ_{targ} [10^{22}s^{-1}]	code	1.34	1.3	1.0	1.2	2.1	2.5
Total D_α	expt.	4.5	3.6	4.7	3.0	10-17	7-14
[10^{20}s^{-1}]	code	4.8	3.9	2.2	2.4	5.5	5.7
Horiz. D_α	expt.	1.68		1.86		2.3-2.8	
[10^{18}m^{-2}s^{-1}]	code	0.56		0.47		0.95	

Table III: Summary of code input parameters for figures 4 - 6.

	OH		H*		H^{RO}
	diff.	pinch	diff.	pinch	pinch
P_e [MW]	0.9	0.9	0.1	0.4	0.5
P_i [MW]	0.9	0.9	7	7	12
P_{RAD} [MW]	0.2	0.2	0.5	0.5	0.8
n_{es} [$10^{19}m^{-3}$]	0.6	0.55	0.7	0.5	0.85
$D_\perp$ [m^2/s]	0.03	0.1	0.015	0.1	0.1
$v_{pinch}/D_\perp$ [m^{-1}]	–	15	–	45	25
χ_e [m^2/s]	0.5-2		0.7-3		0.5-3
χ_i [m^2/s]	1.0		1.0		1.0

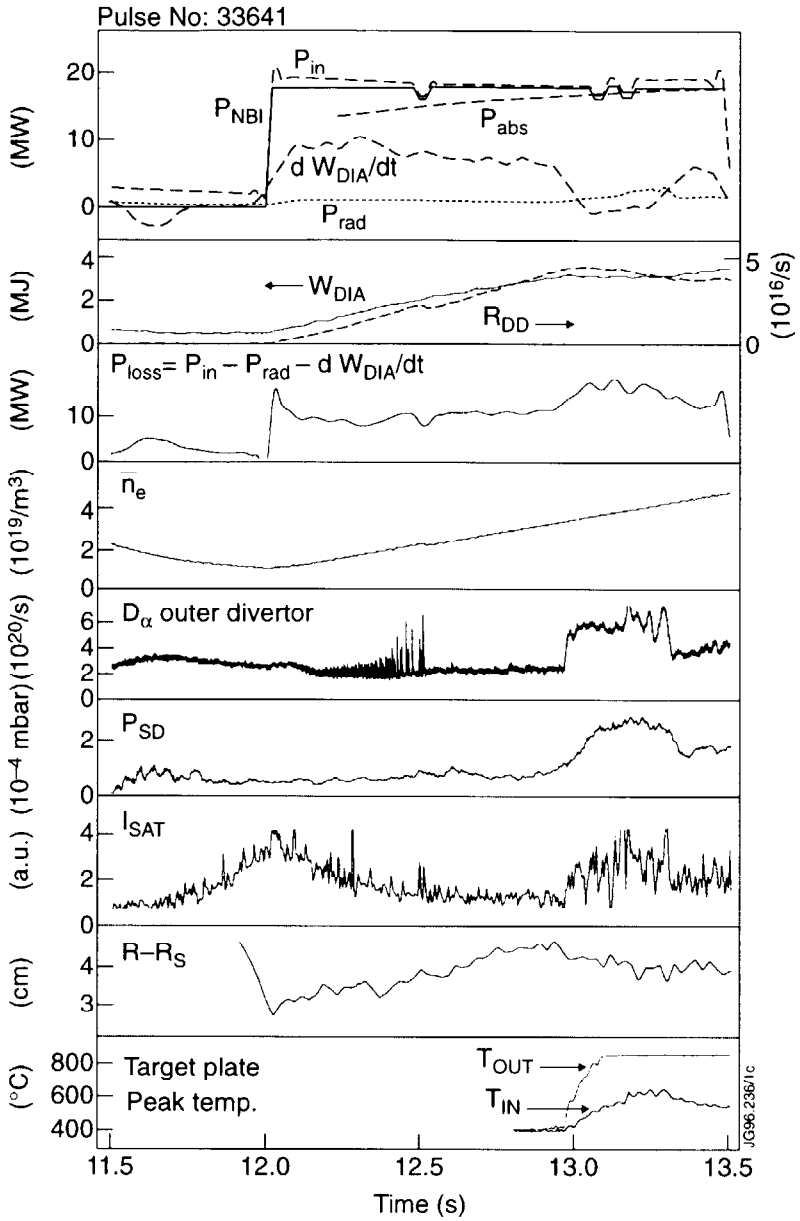

Fig.1: Time traces for global (top four boxes) and divertor parameters. Shot #33641.

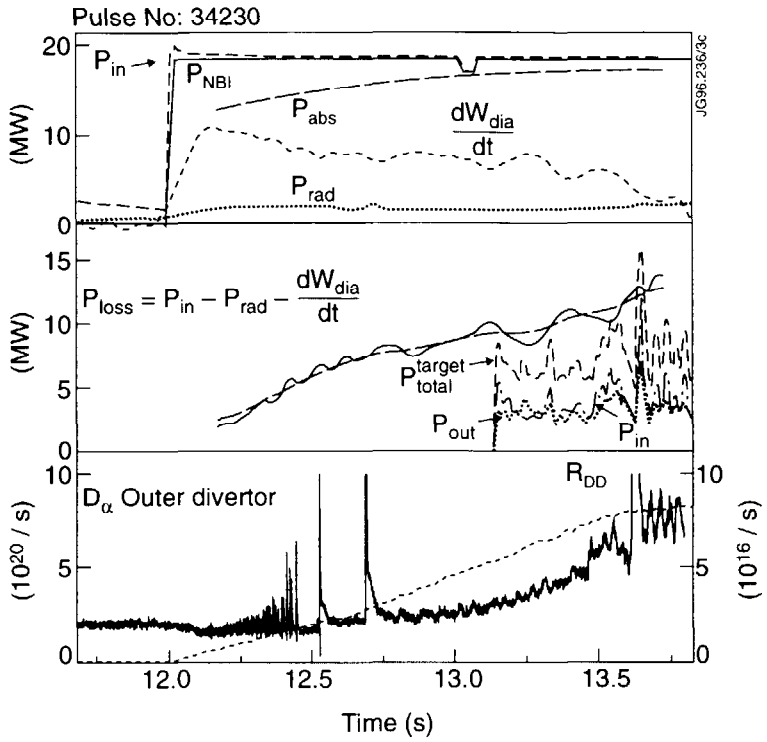

Fig.2: #34230, P_{in} = P_{NBI} + P_{OH}; P_{abs} = absorbed NBI power (calculated). P_{LOSS} = P_{abs} + P_{OH} - dW_{dia}/dt - P_{RAD} (The dashed line gives the time-averaged value). Inner and outer target plate power loading, deduced from IR camera measurements. D_α from the entire outer target plate.

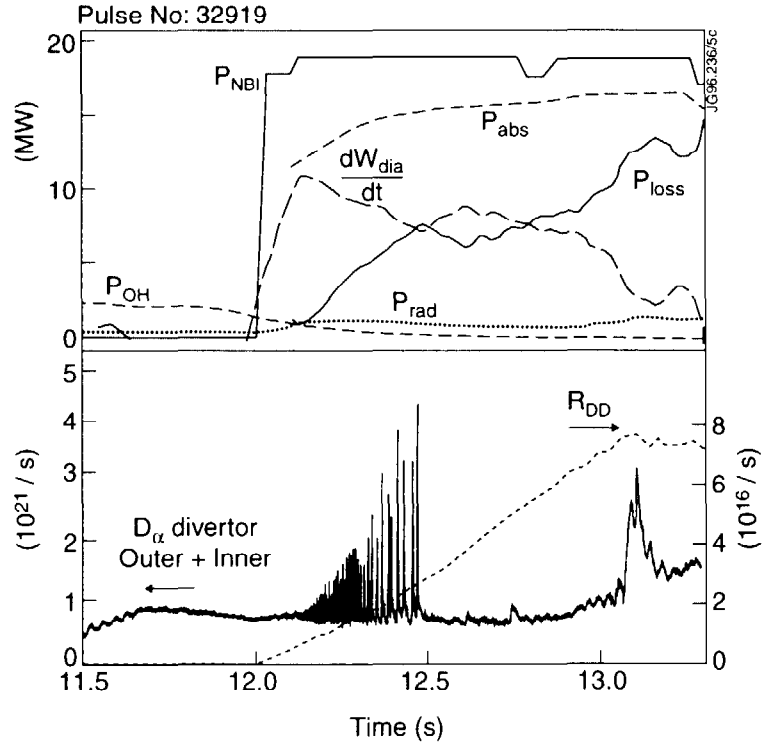

Fig.3: Global parameters for #32919.

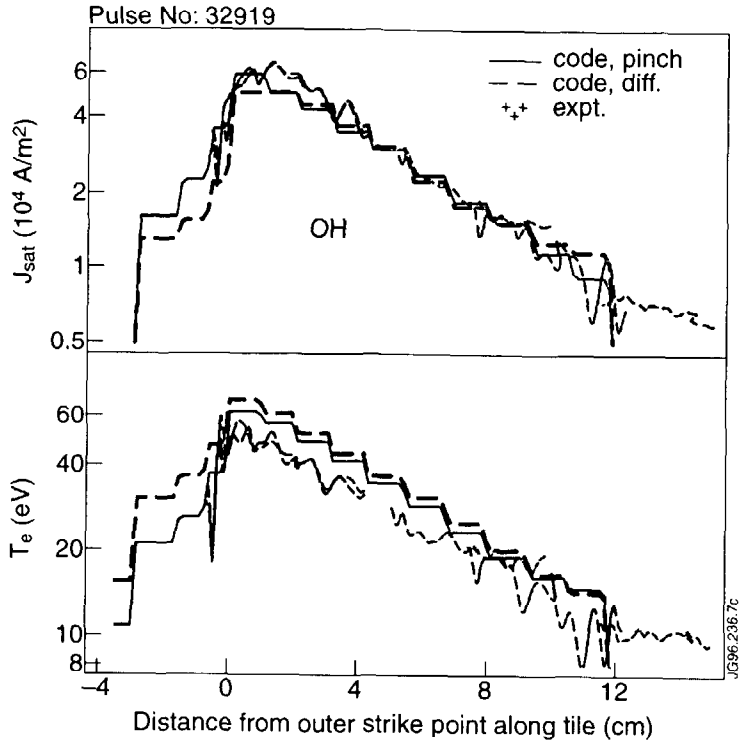

Fig. 4: Experimental J_{sat} and T_e-profiles at the outer target plate for the ***OH phase*** *(51.75-52.0 sec); and the modelled results using diffusion alone, or with a pinch. INPUT: $P_e = P_i = 0.9$ MW, $P_{RAD} = 0.2$MW; $n_{es} = 0.6 \times 10^{19}$ m^{-3} (no pinch), $n_{es} = 0.55 \times 10^{19}$ m^{-3} (pinch); $D_\perp = 0.03$ m^2/s (no pinch), $D_\perp = 0.1$ m^2/s, $v_{pinch} = -1.5$ m/s ($v_{pinch}/D_\perp = 15$); $\chi_e \sim 0.5 - 2$ m^2/s, $\chi_i = 1$ m^2/s.*

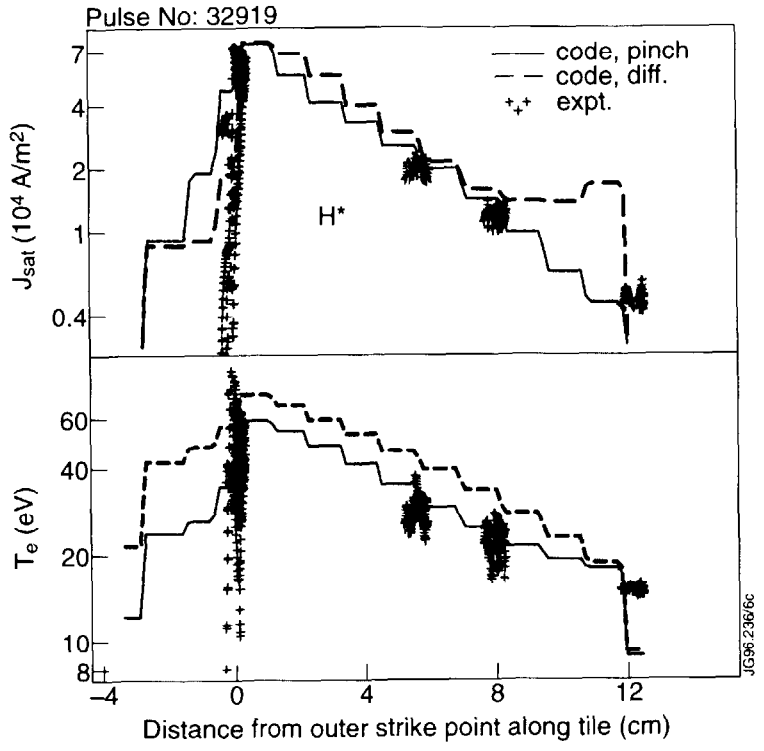

Fig. 5: Experimental J_{sat} and T_e-profiles at the outer target plate for the ***high performance phase, H**** *(52.55-52.9 sec); and the modelled results using diffusion alone, or with a pinch. INPUT: P_e = 0.1 MW (no pinch), P_e = 0.4MW (pinch); P_i = 7 MW, P_{RAD} = 0.5MW; n_{es} = 0.7 x10^{19} m^{-3} (no pinch); n_{es} = 0.5 x10^{19} m^{-3} (pinch); $D_\perp$ = 0.015 m^2/s (no pinch), $D_\perp$ = 0.1 m^2/s, v_{pinch} = -4.5 m/s ($v_{pinch}/D_\perp$= 45); χ_e ~ 0.7 - 3 m^2/s, χ_i = 1 m^2/s.*

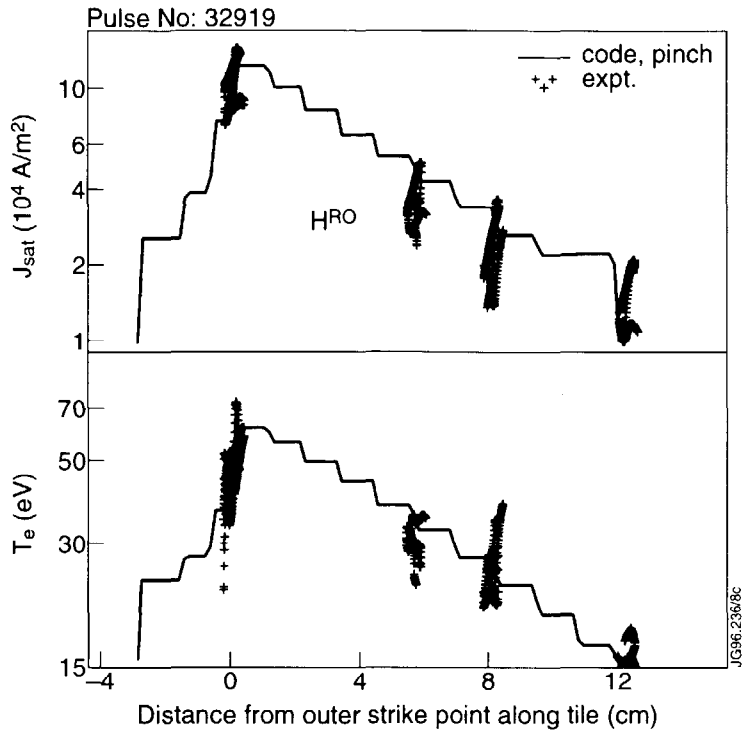

Fig. 6: Experimental J_{sat} and T_e-profiles at the outer target plate for the ***rollover phase*** H^{RO} *(53.1-53.2 sec), and modelled results using diffusion with a pinch. INPUT:* P_e = 0.5 *MW,* P_i = 12*MW,* P_{RAD} = 0.8*MW;* $n_{es} = 0.85 \times 10^{19}\ m^{-3}$, $D_\perp = 0.1\ m^2/s$, v_{pinch} = -2.5 *m/s* ($v_{pinch}/D_\perp$ = 25); $\chi_e \sim 0.5 - 3.0\ m^2/s$, $\chi_i = 1\ m^2/s$.